

Deriving 3D Functional Brain Regions from Multi-Slice Functional Ultrasound Data Using ICA and IVA

Lehmann, Isabell; Adali, Tulay ; Kruizinga, Pieter; Hunyadi, Bori

DOI

[10.1109/IEEECONF59524.2023.10477081](https://doi.org/10.1109/IEEECONF59524.2023.10477081)

Publication date

2023

Document Version

Final published version

Published in

Proceedings of the 2023 57th Asilomar Conference on Signals, Systems, and Computers

Citation (APA)

Lehmann, I., Adali, T., Kruizinga, P., & Hunyadi, B. (2023). Deriving 3D Functional Brain Regions from Multi-Slice Functional Ultrasound Data Using ICA and IVA. In *Proceedings of the 2023 57th Asilomar Conference on Signals, Systems, and Computers* (pp. 1484-1490). IEEE.
<https://doi.org/10.1109/IEEECONF59524.2023.10477081>

Important note

To cite this publication, please use the final published version (if applicable).
Please check the document version above.

Copyright

Other than for strictly personal use, it is not permitted to download, forward or distribute the text or part of it, without the consent of the author(s) and/or copyright holder(s), unless the work is under an open content license such as Creative Commons.

Takedown policy

Please contact us and provide details if you believe this document breaches copyrights.
We will remove access to the work immediately and investigate your claim.

Green Open Access added to TU Delft Institutional Repository

'You share, we take care!' - Taverne project

<https://www.openaccess.nl/en/you-share-we-take-care>

Otherwise as indicated in the copyright section: the publisher is the copyright holder of this work and the author uses the Dutch legislation to make this work public.

DERIVING 3D FUNCTIONAL BRAIN REGIONS FROM MULTI-SLICE FUNCTIONAL ULTRASOUND DATA USING ICA AND IVA

Isabell Lehmann¹, Tülay Adalı², Pieter Kruizinga³, Borbála Hunyadi⁴

¹ Signal and System Theory Group, Paderborn University, Germany

² Dept. of CSEE, University of Maryland, Baltimore County, Baltimore, MD, USA

³ Department of Neuroscience, Erasmus MC, Netherlands

⁴ Signal Processing Systems, TU Delft, Netherlands

ABSTRACT

Functional Ultrasound (fUS) is a relatively new modality to measure brain activity with a high spatio-temporal resolution. In order to collect full-brain information with this 2D imaging technique, fUS data is typically collected for a fixed position of the ultrasound probe for the duration of the experiment, before the probe is moved to the next position. As a result, a 3D functional volume consists of subsequent, time-disjunct 2D datasets. The gold-standard way to analyze fUS datasets is using correlation images or a general linear model. However, these analyses are performed slice by slice; thus, common information across slices is not exploited. We propose the use of two data-driven models, Independent Component Analysis (ICA) and its multiset extension Independent Vector Analysis (IVA), in order to map the mouse visual information processing pathway in 3D. We demonstrate the successful application of ICA and then of IVA, which leverages the dependence across slices in a unique fashion. Furthermore, we provide guidance as to when which approach might be desirable.

Index Terms— functional ultrasound, multi-slice, blind source separation, data-driven, independent component analysis, independent vector analysis

1. INTRODUCTION

Functional Ultrasound (fUS) is a relatively new invasive modality for measuring the cerebral blood volume in the brain, first introduced in 2011 [1]. Because of neurovascular coupling, an increase in blood flow and/or volume can be linked to increased neural activity [1]. Thus, fUS can be used to infer brain activity. Compared to the gold-standard method for measuring brain activity, functional Magnetic Resonance Imaging (fMRI), fUS has a higher spatio-temporal resolution: the spatial resolution of fUS is 50 – 350 μm compared to 1 – 3 mm in fMRI, and the temporal resolution is 4 – 10 Hz for fUS and 0.3 – 1 Hz for fMRI, respectively [2, 3]. Typically, fUS data is collected in a 2D imaging plane, i.e., several 2D images are collected over time for a fixed position of the ultrasound probe before the probe is moved. The gold standard to analyze multi-slice fUS data is using correlation images or a General Linear Model (GLM) approach [3]. However, besides the fact that this slice-by-slice analysis is not mak-

ing use of the dependence across datasets, it was shown in previous work [4] that the brain response strength varies a lot across consecutive stimuli, so a correlation/GLM may be too rigid and cannot capture this variability. Furthermore, these methods can only be applied if the data is collected during a task experiment and the expected stimuli responses for the task are known. Therefore, they are not feasible for analyzing resting state data, which is of great importance to obtain information about the functional organization of the brain [5, 6].

In this paper, we investigate the use of Independent Component Analysis (ICA), a well-known matrix decomposition technique, and Independent Vector Analysis (IVA), the multiset extension of ICA, for analyzing multi-slice fUS data in a fully data-driven way, i.e., without the need of prior information. The use of data-driven analysis using Singular Value Decomposition (SVD) or ICA for retrieving functional networks [7] or Regions Of Interest (ROIs) [4, 8] within a single slice has become more popular in recent years. Very recently, ICA has also been used to map whole-brain mouse functional connectivity from novel 3D recordings [9] and for slice-by-slice evaluation of consecutive 2D recordings [10]. However, in the latter case, ICA does not exploit the information that is common across the slices. Therefore, in this paper, we propose the use of IVA for mapping the mouse visual information processing pathway in 3D, i.e., tracking the estimated ROIs over multiple 2D slices. The pre- and postprocessing of the data before applying these methods is very important but not straight-forward and will be explained in this work. By evaluating ICA and IVA on a multi-slice fUS dataset collected during an experiment with visual stimuli at different locations, we show that these methods can estimate similar ROIs as found by correlation images, without prior knowledge about the experiment design.

2. METHODS

2.1. Correlation images

The gold standard for identifying functional (active) brain regions in task data is to use correlation images [5]. For each slice, a correlation image for each stimulus pattern can be calculated. The value of each pixel in a correlation image is the

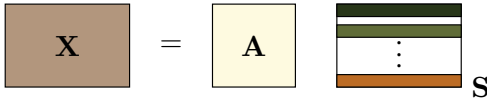


Fig. 1: Illustration of the ICA model. Different colors in the source matrix \mathbf{S} correspond to the independent source components.

correlation of the time course of that pixel with the expected stimulus response $e(t)$, where the expected stimulus response is the time course of the stimulus $c(t)$ convolved with the Hemodynamic Response Function (HRF) $h(t)$:

$$e(t) = c(t) * h(t). \quad (1)$$

In our case, we model the HRF by a shifted Dirac impulse function:

$$h(t) = \delta(t - t_0), \quad (2)$$

where t_0 denotes the shift in time. The pixels with high correlation values correspond to the brain regions that are activated by the corresponding stimulus.

2.2. Independent Component Analysis

ICA [11] is a matrix decomposition-based model to estimate latent sources from observed data. The generative model of ICA is shown in Figure 1 and is denoted as

$$\mathbf{X} = \mathbf{A}\mathbf{S}, \quad (3)$$

where $\mathbf{X} \in \mathbb{R}^{R \times N}$ is the observed data matrix, $\mathbf{S} \in \mathbb{R}^{R \times N}$ is the unknown source matrix, $\mathbf{A} \in \mathbb{R}^{R \times R}$ is an unknown invertible mixing matrix, R is the dimension of the data, and N is the number of samples. ICA assumes the source components $\mathbf{s}_{r \cdot} \in \mathbb{R}^{1 \times N}$, i.e., the rows of \mathbf{S} , to be independent of each other, which is visualized by the different colors in Figure 1.

The goal of ICA is now to estimate the sources

$$\hat{\mathbf{S}} = \mathbf{W}\mathbf{X}, \quad (4)$$

where $\mathbf{W} \in \mathbb{R}^{R \times R}$ is the estimated demixing matrix. Different methods exist for estimating the sources in ICA. In this work, we choose the commonly used FastICA algorithm [11] that is based on maximization of negentropy, implemented in `scikit-learn` [12]. We run ICA 20 times with random initializations and choose the most consistent run [13].

2.3. Independent Vector Analysis

IVA [14] is an extension of ICA to multiple datasets. The generative model of IVA, shown in Figure 2, is

$$\mathbf{X}^{[k]} = \mathbf{A}^{[k]}\mathbf{S}^{[k]}, \quad k = 1, \dots, K, \quad (5)$$

where $\mathbf{X}^{[k]} \in \mathbb{R}^{R \times N}$ is the observed data in the k^{th} dataset, $\mathbf{S}^{[k]} \in \mathbb{R}^{R \times N}$ is the source matrix in the k^{th} dataset, and

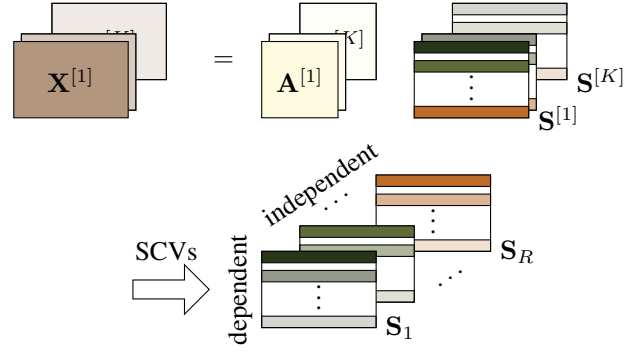


Fig. 2: Illustration of the IVA model. Different colors in the sources matrices $\mathbf{S}^{[k]}$ correspond to independent source components, while different opacities of the same color indicate dependent source components. The r^{th} SCV is formed by stacking the r^{th} row of all K source matrices together.

$\mathbf{A}^{[k]} \in \mathbb{R}^{R \times R}$ is the mixing matrix of the k^{th} dataset. IVA now aims to jointly estimate the sources

$$\hat{\mathbf{S}}^{[k]} = \mathbf{W}^{[k]}\mathbf{X}^{[k]}, \quad k = 1, \dots, K, \quad (6)$$

where $\mathbf{W}^{[k]} \in \mathbb{R}^{R \times R}$ is the demixing matrix for the k^{th} dataset.

As ICA, also IVA assumes the source components within a source to be independent, but additionally aims to make use of the dependence of sources across datasets whenever such dependence exists [15]. This is achieved by introducing so-called Source Component Vectors (SCVs). Let the r^{th} SCV $\mathbf{S}_r \in \mathbb{R}^{K \times N}$ be defined by stacking the r^{th} source component of all datasets [15]:

$$\mathbf{S}_r = \left[\left(\mathbf{s}_{r \cdot}^{[1]} \right)^{\top} \dots \left(\mathbf{s}_{r \cdot}^{[K]} \right)^{\top} \right]^{\top}, \quad (7)$$

where $\mathbf{s}_{r \cdot}^{[k]} \in \mathbb{R}^{1 \times N}$ is the r^{th} row of the k^{th} dataset. In Figure 2, dependence of source components is indicated by different opacities of the same color. As we see, the (potentially) dependent source components are stacked into an SCV, and the source components among SCVs are independent of each other.

In order to maximize independence among the estimated SCVs, IVA now minimizes their Mutual Information (MI), which is defined as [14, 15]

$$I(\mathbf{W}^{[k]}) = \left(\sum_{r=1}^R H(\hat{\mathbf{S}}_r) - \sum_{k=1}^K \log \left| \det(\mathbf{W}^{[k]}) \right| - C \right),$$

where $H(\hat{\mathbf{S}}_r)$ is the (differential) entropy of the r^{th} estimated SCV, and C is a constant.

In this work, we use IVA-G [16], which assumes a multivariate Gaussian distribution as a model for the probability density function of the SCVs. Therefore, IVA-G takes only second-order statistics into account, and the source components within an SCV are made maximally correlated and

across SCVs maximally uncorrelated.¹ We choose the most consistent of 20 runs [13].

3. EXPERIMENTS

3.1. Dataset

fUS imaging data is collected from a head-fixed mouse on a wheel, which is looking at two screens. During the experiment, black-and-white flickerings occurred on 9 different locations on the screens. The flickering at each location is called a stimulus; thus, there are 9 different stimuli in this experiment. The stimuli occur in a pseudo-random order, where each stimulus is presented five times. The stimulus duration is 2.92 seconds, and the duration of the breaks between stimuli is between 7.52 and 10.88 seconds. After collecting the Power Doppler Images (PDIs) over T time points (with a sampling frequency $f_s = 4.65$ Hz) for a fixed probe position, the probe is moved to a different position, and the experiment is repeated. The order of the stimulus occurrences is the same for each probe position. We use data collected from the following probe positions (distance from Bregma): -3.16 mm, -3.36 mm, -4.26 mm, -4.56 mm, -4.76 mm, -4.96 mm. Thus, for each probe position, one slice of the brain is captured, and in total we have $K = 6$ datasets. We denote the data of the k^{th} slice as a tensor $\mathcal{X}^{[k]} \in \mathbb{R}^{N_z \times N_x \times T}$, where $N_z = 150$ and $N_x = 256$ are the numbers of pixels in the z and x direction, respectively, and $T = 2530$ is the number of time points over which data is collected.

This experiment, by virtue of its simplicity, enables us to easily demonstrate and evaluate the performance of ICA and IVA, by comparing their results with the correlation images and interpreting the identified ROIs.

3.2. Preprocessing

The following preprocessing is applied to the PDIs of each slice $k = 1, \dots, K$ separately. In the following explanation, we drop the slice index k for better readability.

1. (a) For correlation images: image standardization: The image for each time point t , $\mathcal{X}(:, :, t) \in \mathbb{R}^{N_z \times N_x}$, is made zero-mean and unit-variance.
- (b) For ICA/IVA: temporal standardization: Each pixel's time course, $\mathcal{X}(i, j, :) \in \mathbb{R}^T$, is made zero-mean and unit-variance.
2. Spatial smoothing: A 2-dimensional Gaussian filter with $\sigma = 1$ is applied to the image collected for each time point t , $\mathcal{X}(:, :, t) \in \mathbb{R}^{N_z \times N_x}$.
3. Temporal smoothing: A fifth-order Butterworth low-pass filter with a cut-off frequency of 0.2 Hz is applied on each pixel's time course $\mathcal{X}(i, j, :)$.

¹The Python implementation of IVA-G is available at https://github.com/SSTGroup/independent_vector_analysis [17].

The following two steps are only applied for ICA/IVA.

4. Reshaping: The tensor $\mathcal{X} \in \mathbb{R}^{N_z \times N_x \times T}$ is unfolded in a matrix $\tilde{\mathbf{X}} \in \mathbb{R}^{T \times N}$, where $N = N_z N_x$. We treat N as the number of samples and T as the dimension of the data.
5. Dimensionality reduction and whitening: Principal Component Analysis (PCA) is applied to $\tilde{\mathbf{X}}$ to get the matrix $\mathbf{X} = \mathbf{P}^T \tilde{\mathbf{X}}$, where $\mathbf{P} \in \mathbb{R}^{T \times R}$, $R \ll T$, is the PCA transformation matrix. ICA and IVA are then applied to $\mathbf{X} \in \mathbb{R}^{R \times N}$.

3.3. Estimation of ROIs

3.3.1. Correlation images

Correlation images are calculated from the image-standardized, spatially and temporally smoothed tensor $\mathcal{X} \in \mathbb{R}^{N_z \times N_x \times T}$. We choose $t_0 = 7$ samples as time shift in the HRF in (2), which corresponds to approximately 1.75 seconds. The highly correlated pixels in a correlation image form a ROI. We denote the correlation image for the r^{th} stimulus in the k^{th} slice as $\mathbf{C}_r^{[k]} \in \mathbb{R}^{N_z \times N_x}$.

3.3.2. ICA

We assume that the measured data is a mixture of the activity fluctuations of multiple spatially independent functional-anatomical regions. As such, we decompose each dimension-reduced dataset $\mathbf{X}^{[k]} \in \mathbb{R}^{R \times N}$ separately using ICA to get the estimated demixing matrix $\mathbf{W}^{[k]}$ and the estimated source matrices $\tilde{\mathbf{S}}^{[k]} \in \mathbb{R}^{R \times N}$, with $R = 20$, $N = 38400$. The r^{th} source component of the k^{th} dataset, $\mathbf{s}_r^{[k]}$, is reshaped into an image $\mathbf{I}_r^{[k]} \in \mathbb{R}^{N_z \times N_x}$. The significant pixels ($p < 0.01$) in each image form a ROI, and the R ROIs for the k^{th} slice are independent of each other. The mixing matrices $\tilde{\mathbf{A}}^{[k]} \in \mathbb{R}^{T \times R}$ can be reconstructed by multiplying the PCA transformation matrix \mathbf{P} with the inverse of the estimated demixing matrix of ICA $(\mathbf{W}^{[k]})^{-1}$:

$$\tilde{\mathbf{A}}^{[k]} = \mathbf{P}(\mathbf{W}^{[k]})^{-1} \in \mathbb{R}^{T \times R}, \quad (8)$$

and the r^{th} column $\tilde{\mathbf{a}}_r^{[k]}$ is the time course corresponding to the r^{th} ROI in the k^{th} dataset.

The source components in ICA can be estimated up to a permutation, scale and sign ambiguity. We overcome the scale ambiguity by normalizing each row $\mathbf{s}_r^{[k]}$ to unit-variance and multiplying the weight in the corresponding column of the mixing matrix $\tilde{\mathbf{a}}_r^{[k]}$. To overcome the sign ambiguity, we make sure that the majority of the pixels in each ROI is positive or made positive by multiplying the corresponding row of $\tilde{\mathbf{S}}^{[k]}$ and column of $\tilde{\mathbf{A}}^{[k]}$ by -1. To overcome the permutation ambiguity, we manually aligned the 20 components across the 6 slices, which is prone to subjective biases/errors. In the final step, we removed the noise components, and 8 components remained.

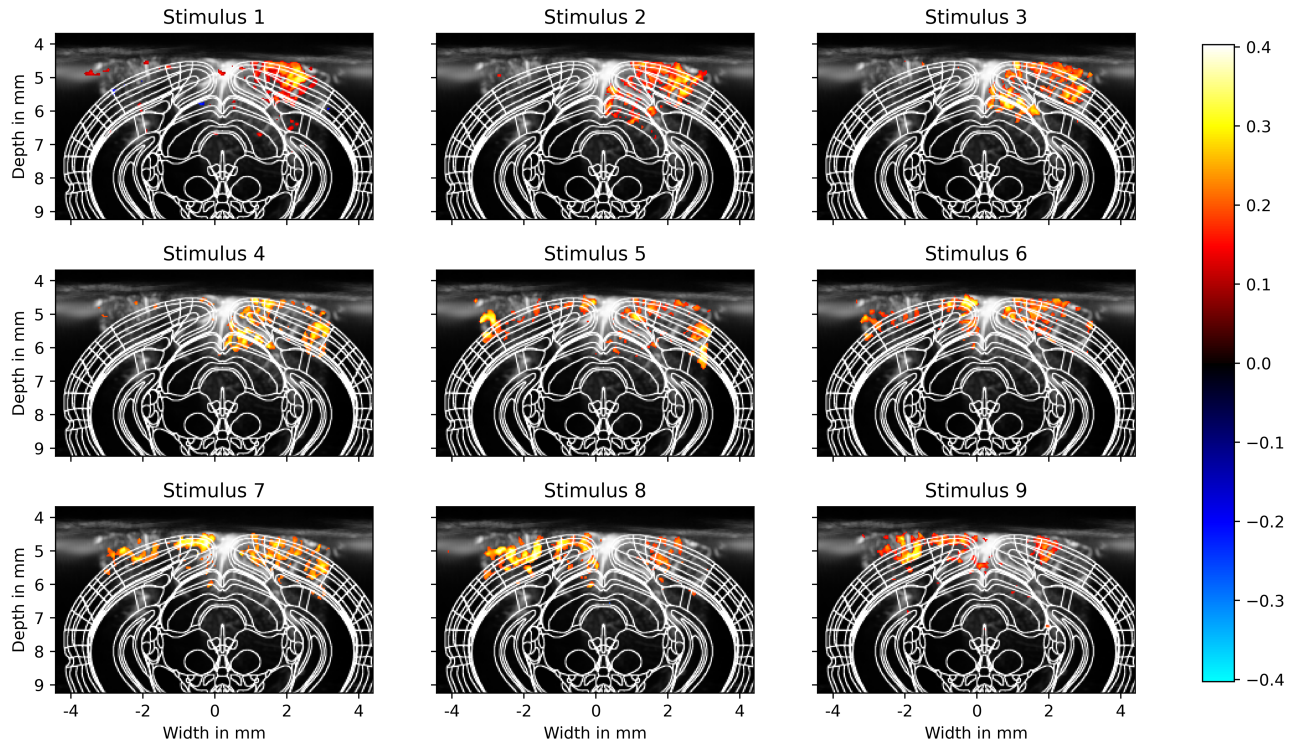


Fig. 3: For probe position -3.36 mm, the location of the stimuli can be tracked in the correlation images: From stimulus 1 to 9 (location most left to most right), we see a movement of the ROIs from right to left.

3.3.3. IVA

IVA is jointly applied on the K dimension-reduced datasets $\mathbf{X}^{[k]} \in \mathbb{R}^{R \times N}$. Reconstruction of mixing matrices and solving the scale and sign ambiguity as well as reshaping the source components into images $\mathbf{I}_r^{[k]}$ is performed in the same way as for ICA. As IVA jointly estimates the sources, the permutation ambiguity is automatically resolved by this method. We match the estimated IVA components to the selected ICA components to be able to compare the results of the methods.

3.3.4. Visualization

For visualization purposes, we calculate the (scalar) mean $\mu_r^{[k]}$ and standard deviation $\sigma_r^{[k]}$ of each image $\mathbf{C}_r^{[k]}$ or $\mathbf{I}_r^{[k]}$, and calculate the z -score of each pixel by subtracting the mean and dividing by the standard deviation. From the resulting z -scored image $\mathbf{Z}_r^{[k]} \in \mathbb{R}^{N_z \times N_x}$, we plot only the significant pixels, i.e., the pixels (i, j) where $|\mathbf{Z}_r^{[k]}(i, j)| > 2.58$, which corresponds to a significance level of $p < 0.01$ for a two-sided t -test.

We overlay the significant pixels over the logarithmic mean image $\mathbf{X}_{\log\text{mean}}^{[k]}$, which is calculated from the raw PDIs (without any preprocessing) for each slice as:

$$\mathbf{X}_{\log\text{mean}}^{[k]} = \log \left(\frac{\mathbf{X}_{\text{mean}}^{[k]}}{\max(\mathbf{X}_{\text{mean}}^{[k]})} \right), \quad (9)$$

where $\mathbf{X}_{\text{mean}}^{[k]} = \sum_{t=1}^T \mathcal{X}^{[k]}(:, :, t)$. Then, we overlay the Allen brain atlas [18] for the corresponding slice so that we can interpret the ROIs in terms of anatomical regions.

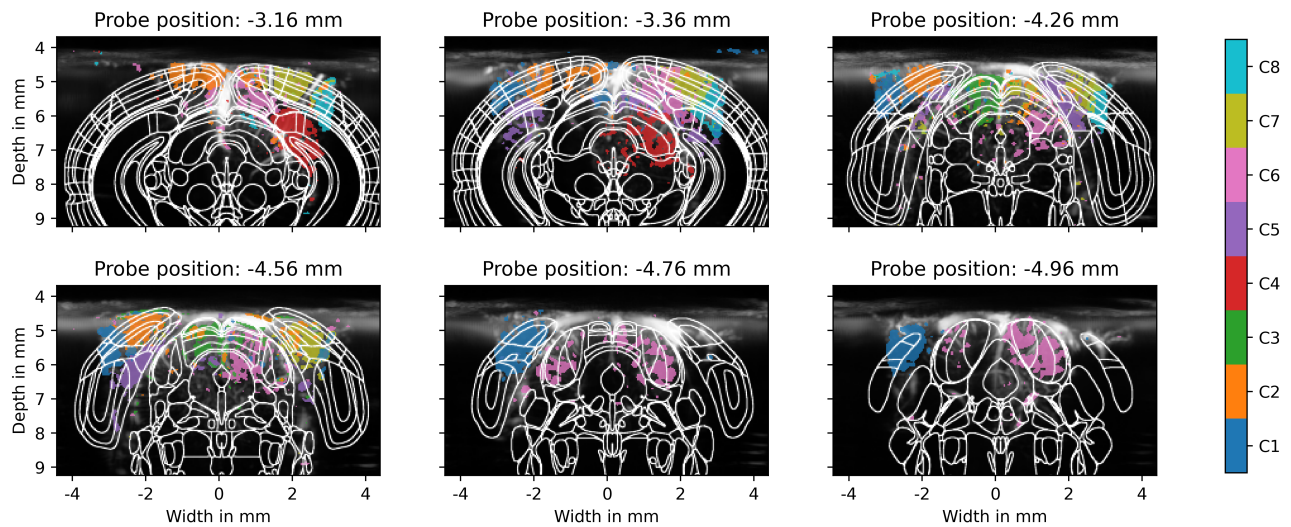
3.4. Results

3.4.1. Correlation images

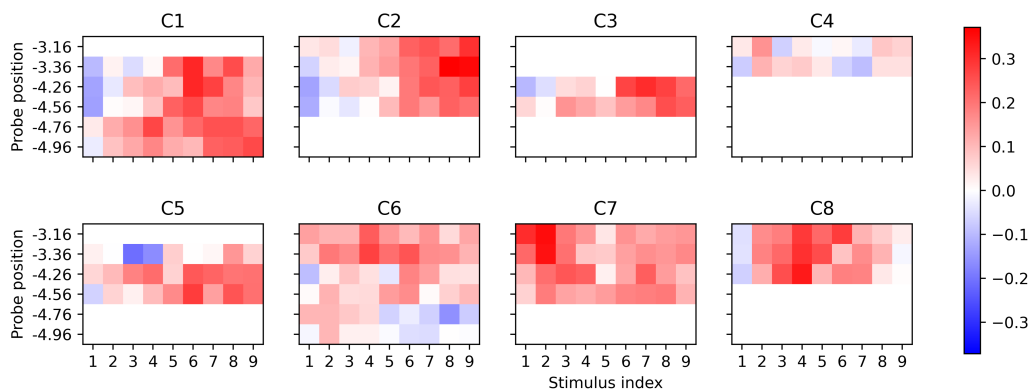
Figure 3 shows the correlation images of probe position -3.36 mm for the 9 stimuli. In the following, we link the ROIs to the anatomical regions defined in the Allen brain atlas [18]. We see positive correlations mainly in V1 on the right side of the brain with stimuli 1–4 and on the left side with stimuli 8–9, which make sense as V1 is part of the visual pathway with contra-lateral activation. For stimuli 5–7, we see the movement of the V1 and RSG ROIs from right to left. Thus, the location of the stimulus can be visually tracked in the correlated brain regions for probe positions -3.36 mm (and also for -4.26 mm and -4.56 mm, which are not shown).

3.4.2. ICA results

Figure 4(a) shows the ROIs estimated by ICA for the 6 probe positions. All ROIs for one slice are plotted in the same image. To distinguish between them, each ROI is plotted in a different color. Furthermore, a component that occurs in multiple slices (as identified manually) is plotted in the same color for each slice. Figure 4(b) shows the correlation of the



(a) ROIs estimated by ICA for the 6 probe positions. Each ROI is plotted in a different color within a slice, and corresponding ROIs are plotted in the same color across slices.



(b) Correlation of ICA time courses and expected stimuli responses.

Fig. 4: ICA results. The ROIs of C1/C2 and C7 belong to the left and right V1, respectively. The time course of C1/C2 is higher correlated with the stimuli on the right side, and the time course of C7 is higher correlated with the stimuli on the left side.

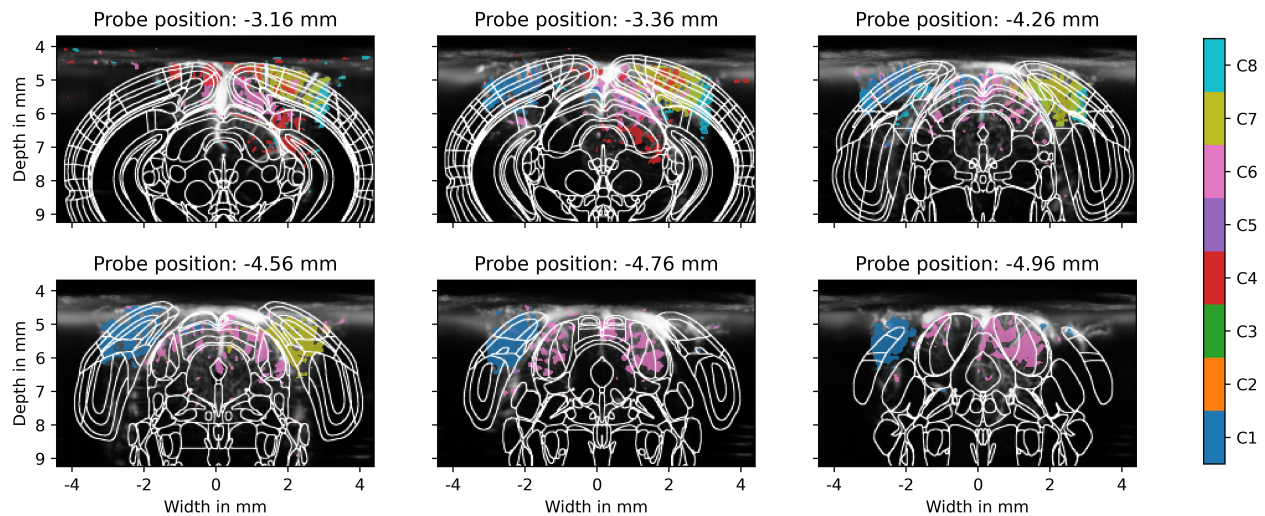
ICA time courses (corresponding to the ROIs in Figure 4(a)) with the 9 expected stimuli responses. If a component is not present in a slice, the corresponding row is empty.

The estimated ROIs correspond to meaningful anatomical brain regions. Component 1 (C1) (dark blue) belongs mainly to the left V1 for probe positions -3.36 mm, -4.26 mm, -4.56 mm, -4.76 mm and -4.96 mm. The corresponding time courses of C1 are higher correlated with the stimuli located on the right side of the screen (stimuli 6–9), which makes sense as the ROI is also present in the correlation images for those stimuli. C2 (orange) corresponds to left V2ML, V2MM, and RSA/RSG at -3.16 mm, and then evolves to mainly activations of V1 (shared with C1) at -3.36 mm to -4.56 mm. Also for the time courses corresponding to this component, we see higher correlations with the stimuli on the right. C5 (purple) belongs to left S (-3.36 mm), left and right PrS (-4.26 mm) and left PrS (-4.56 mm). C7 (olive) shows activations of right V2ML and right V1 (at -3.16 mm) and then mainly right V1

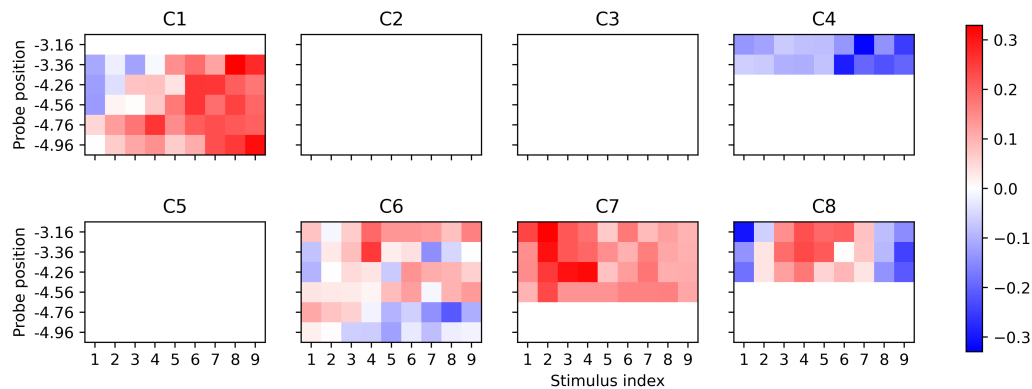
at -3.52 mm to -4.56 mm. The corresponding time course is higher correlated with the stimuli on the left.

3.4.3. IVA results

In Figure 5(a), we see the estimated ROIs of IVA for each slice, and in Figure 5(b), we see the correlation of the IVA time courses with the expected stimuli responses. We can directly see that C1 and C2 in ICA at -3.36 mm to -4.56 mm are merged in C1 in IVA, which makes more sense as they belong to the same anatomical region (left V1) and again reflect the contra-lateral activation of the visual pathway. However, C3 and C5 are completely missing in IVA. C7 and C8 are very similar for ICA and IVA, and also the ROIs of C1 and C6 for probe positions -4.76 mm and -4.96 mm look almost identical for both methods. The time courses of C1 (left side of brain) are again higher correlated with the right stimuli, and the time courses of C7



(a) ROIs estimated by IVA for the 6 probe positions. Each ROI is plotted in a different color within a slice, and corresponding ROIs are plotted in the same color across slices.



(b) Correlation of IVA time courses and expected stimuli responses.

Fig. 5: IVA results. The ROIs of C1 and C7 belong to the left and right V1, respectively. The time course of C1 is higher correlated with the stimuli on the right side, and the time course of C7 is higher correlated with the stimuli on the left side. The time courses of C4, where the ROIs belong to RSA/RSG, are anti-correlated with all stimuli.

(right side of brain) higher with the left stimuli. We see a strong negative correlation of the time course of C4 with all stimuli, which is not present in ICA. The activations of C4 in the RSA/RSG regions for probe positions -3.16 mm and -3.36 mm, which are associated with the mouse default mode, do not correspond to C4 but to C2 in ICA. Thus, IVA seems to extract the default mode network, which ICA seems to merge with another component.

4. DISCUSSION

We have proposed the use of ICA and IVA to track the 3D visual information processing pathway in multi-slice 2D fUS imaging data. We demonstrated the suitability of these two methods by showing that the identified funcio-anatomical regions match the activations in the correlation images for our specific task dataset. Furthermore, we have shown that the

ICA/IVA time courses of the estimated ROIs are correlated with the expected stimuli responses of those stimuli for which the corresponding ROI is present in the correlation images.

In terms of comparison of the methods ICA and IVA, IVA has the clear advantage of automatically aligning the identified ROIs for the different slices by making use of their dependence when estimating them. However, because IVA aims to make the components dependent across all slices, it tends to miss components that are present only in a few slices. On the other hand, ICA might split or merge ROIs. Choosing the proper analysis method involves a trade-off between obtaining a detailed understanding and minimizing the amount of time spent. We suggest the use of IVA if one is interested in tracking the ROIs over slices and finds it acceptable if ROIs may be missed, and the use of ICA if one is interested to identify as many ROIs as possible while taking the risk that one ROI might be split in two components.

As we have demonstrated the successful application of ICA and IVA for multi-slice fUS task data, the next step can be to analyze resting state data using one of these two methods, where the gold standard of correlation images cannot be used as there is no expected stimulus response. Furthermore, instead of IVA-G, IVA-L-SOS [19] can be used to estimate the sources, as it takes also higher-order statistics into account and thus does not only look at correlations like IVA-G does. Lastly, the quality of the estimated components can be automatically determined by, e.g., analyzing which percentage of pixels in a brain region according to the atlas is significant.

5. ACKNOWLEDGEMENTS

This work was supported in part by the Delft Technology Fellowship, and in part by the German Research Foundation (DFG) under grant SCHR 1384/3-2, and in part by grant NSF 2316420, and in part by the NWO-Groot grant of The Dutch Organization for Scientific Research (Grant no. 108845), awarded to CUBE.

6. REFERENCES

- [1] E. Macé, G. Montaldo, I. Cohen, et al., “Functional ultrasound imaging of the brain,” *Nature Methods*, vol. 8, no. 8, pp. 662–664, 2011.
- [2] M. Markicevic, I. Savvateev, C. Grimm, and V. Zerbi, “Emerging imaging methods to study whole-brain function in rodent models,” *Translational Psychiatry*, vol. 11, no. 1, 2021.
- [3] C. Brunner, M. Grillet, A. Urban, et al., “Whole-brain functional ultrasound imaging in awake head-fixed mice,” *Nature Protocols*, vol. 16, no. July, pp. 3547–3571, 2021.
- [4] A. Erol, C. Soloukey, B. Generowicz, et al., “Deconvolution of the Functional Ultrasound Response in the Mouse Visual Pathway Using Block-Term Decomposition,” *Neuroinformatics*, pp. 1–19, 2022.
- [5] A. Urban, C. Dussaux, G. Martel, et al., “Real-time imaging of brain activity in freely moving rats using functional ultrasound,” *Nature Methods*, vol. 12, no. 9, pp. 873–878, 2015.
- [6] P. Pais-Roldán, C. Mateo, W. J. Pan, et al., “Contribution of animal models toward understanding resting state functional connectivity,” *NeuroImage*, vol. 245, no. September, 2021.
- [7] B. F. Osmanski, S. Pezet, A. Ricobaraza, Z. Lenkei, and M. Tanter, “Functional ultrasound imaging of intrinsic connectivity in the living rat brain with high spatiotemporal resolution,” *Nature Communications*, vol. 5, 2014.
- [8] R. Wijnands, J. Dauwels, I. Serra, et al., “Modeling and inference of sparse neural dynamic functional connectivity networks underlying functional ultrasound data,” in *2023 IEEE International Conference on Acoustics, Speech, and Signal Processing Workshops (ICASSPW)*. IEEE, 2023, pp. 1–5.
- [9] K. Hikishima, T. Tsurugizawa, K. Kasahara, et al., “Brain-wide mapping of resting-state networks in mice using high-frame rate functional ultrasound,” *NeuroImage*, vol. 279, pp. 120297, 2023.
- [10] A. Bertolo, J. Ferrier, S. Cazzanelli, et al., “High sensitivity mapping of brain-wide functional networks in awake mice using simultaneous multi-slice fus imaging,” *Imaging Neuroscience*, vol. 1, pp. 1–18, 2023.
- [11] A. Hyvärinen and E. Oja, “Independent component analysis: algorithms and applications,” *Neural Networks*, vol. 13, no. 4, pp. 411–430, 2000.
- [12] F. Pedregosa, G. Varoquaux, A. Gramfort, et al., “Scikit-learn: Machine learning in Python,” *Journal of Machine Learning Research*, vol. 12, pp. 2825–2830, 2011.
- [13] Q. Long, C. Jia, Z. Boukouvalas, et al., “Consistent Run Selection for Independent Component Analysis: Application to fMRI Analysis,” *ICASSP, IEEE International Conference on Acoustics, Speech and Signal Processing - Proceedings*, pp. 2581–2585, 2018.
- [14] T. Kim, T. Eltoft and T.-W. Lee, “Independent vector analysis: An extension of ICA to multivariate components,” *International conference on independent component analysis and signal separation*, pp. 165–172, 2006.
- [15] T. Adali, M. Anderson and G. S. Fu, “Diversity in independent component and vector analyses: Identifiability, algorithms, and applications in medical imaging,” *IEEE Signal Processing Magazine*, vol. 31, no. 3, pp. 18–33, 2014.
- [16] M. Anderson, T. Adali and X.-L. Li, “Joint blind source separation with multivariate Gaussian model: Algorithms and performance analysis,” *IEEE Transactions on Signal Processing*, vol. 60, no. 4, pp. 1672–1683, 2012.
- [17] I. Lehmann, E. Acar, T. Hasija, et al., “Multi-task fMRI Data Fusion Using IVA and PARAFAC2,” in *2022 IEEE International Conference on Acoustics, Speech and Signal Processing*, 2022, pp. 1466–1470.
- [18] Q. Wang, S.-L. Ding, Y. Li, et al., “The Allen mouse brain common coordinate framework: a 3D reference atlas,” *Cell*, vol. 181, no. 4, pp. 936–953, 2020.
- [19] S. Bhinge, R. Mowakeaa, V. D. Calhoun, and T. Adali, “Extraction of Time-Varying Spatiotemporal Networks Using Parameter-Tuned Constrained IVA,” *IEEE Transactions on Medical Imaging*, vol. 38, no. 7, pp. 1715–1725, 2019.